

MEASURING INTER-HEMISPHERIC INTEGRATION IN BIPOLAR AFFECTIVE DISORDER USING BRAIN NETWORK ANALYSES AND HARDI

A. Leow^{1,2}, L. Zhan⁴, O. Ajilore¹, J. GadElkarim^{1,3}, A. Zhang¹,
D. Arienzo⁵, T. Moody⁵, J. Feusner⁵, A. Kumar¹, P. Thompson⁴, L. Altshuler⁵

¹ Department of Psychiatry, UIC, Chicago, IL

² Department of Bioengineering, UIC, Chicago, IL

³ Department of Electrical & Computer Engineering, UIC, Chicago, IL

⁴ LONI, Department of Neurology, UCLA, Los Angeles, CA

⁵ Department of Psychiatry, UCLA, Los Angeles, CA

ABSTRACT

Bipolar disorder is characterized by extreme mood swings, including both manic and depressive episodes commonly accompanied by psychosis. Many imaging studies have investigated white matter changes in bipolar illness, and the results have suggested abnormal intra- and inter-hemispheric white matter structures, particularly in the fronto-limbic and callosal systems. However, some inconsistency remains in the literature, and no study to-date has utilized brain network analysis using graph theory. Here, we acquired 64-direction diffusion weighted imaging (DWI) on 25 euthymic bipolar I subjects and 25 gender/age matched healthy subjects. White matter integrity measures were computed and compared in 50 white matter ROIs. The results indicated impaired integrity in the corpus callosum. Guided by this, we constructed whole brain structural connectivity networks using graph theory. We devised brain network metrics (inter-hemispheric path length and efficiency) to further probe inter-hemispheric integration, and demonstrated relatively preserved intra-hemispheric but significantly impaired inter-hemispheric integration in our bipolar subjects.

Index Terms— bipolar disorder, diffusion imaging, tractography, brain network analysis

1. INTRODUCTION

In graph theory, a network is a set of nodes and the connections between them. The advantage of such approach is that it allows for quantitative analyses of complex brain networks to provide information on organizational systems. Using diffusion tensor imaging, white matter abnormalities have been reported in subjects with bipolar disorder in certain brain regions including prefrontal, parietal, and temporal lobes (for extensive reviews, please see [1~3]). However, no studies to date have investigated bipolar disorder using higher angular resolution diffusion imaging (HARDI) or brain network analysis. Here we present the results of first ever such study. We posit that true white

matter integrity changes will manifest in both standard DTI and HARDI-corrected measures. Thus, any false positive fractional anisotropy or false positive mean diffusivity changes would exhibit no corresponding changes in their HARDI-corrected counterparts. Furthermore, any white matter integrity changes will be further confirmed in the subsequent brain network analysis using graph theory.

2. METHODS

The study protocol was approved by the Institutional Review Boards (IRBs) at both the University of California, Los Angeles and University of Illinois, Chicago. All subjects gave informed consent after having understood all issues pertaining to participation in the study. The sample consisted of 25 participants with bipolar I disorder (14 male and 11 female; age: 41.7 +/-12.6) and 25 healthy controls (n=25; 13 male and 12 female; age: 42.2+/-10.8). All bipolar subjects met the DSM IV criteria for bipolar I disorder, and were euthymic at the time of the study. The two groups did not statistically differ in either gender or age.

2.1. Image acquisition

Diffusion weighted MRI data were acquired on a Siemens 3T Trio scanner. Sixty contiguous axial brain slices were collected using the following parameters: 64 diffusion-weighted ($b=1000$ s/mm²) and 1 non-diffusion weighted scan; FOV: 190mm by 190mm; voxel size: 2x2x2mm; TR=8400ms; TE=93ms. A T1-weighted magnetization-prepared rapid-acquisition gradient echo (MPRAGE) was acquired for registration and segmentation purposes; FOV 250mm by 250 mm; voxel size: 1x1x1mm; TR=1900ms, TE=2.26ms, flip angle=9°.

2.2. Image Processing

To generate DTI white matter measures, all images were first corrected for eddy current distortions using FSL toolbox (<http://fsl.fmrib.ox.ac.uk/fsl>). Next, we used MedINRIA (<http://www-sop.inria.fr/asclepios/software/>) to compute diffusion tensors at each voxel. To construct HARDI-corrected white matter measures, we used the

tensor distribution function [4], a mathematical model that can probabilistically estimate both the number of tensors and their individual anisotropy properties. As a result, standard measures including FA and MD can be decomposed and the confound of white matter subvoxel architecture (e.g., fiber crossing) may be removed.

For each subject, whole brain white matter was parcellated into 50 ROIs (**Table 1**) based on the ICBM young adult DTI-81 atlas (<http://www.loni.ucla.edu/ICBM/>). We first registered atlas FA to individual subject's FA using 12-parameter affine registration to obtain a transformation matrix and then applied the transformation matrix to all atlas white matter ROIs to map them onto the target individual space. White matter integrity measures based on both DTI and HARDI were computed and averaged in each ROI for group comparisons.

Table 1. 50 white matter parcellation ROIs. * indicates tracts that are present in both left and right hemispheres

MCP	Middle cerebellar peduncle	BCC	Body of corpus callosum
PCT	Pontine crossing tract	SCC	Splenium of corpus callosum
ICP*	Inferior cerebellar peduncle	GCC	<i>Genu</i> of corpus callosum
SCP*	Superior cerebellar peduncle	ACR*	Anterior <i>corona radiata</i>
CST*	Corticospinal tract	ML*	Medial lemniscus
PCR*	Posterior <i>corona radiata</i>	PTR*	Posterior thalamic radiation
SS*	Sagittal <i>stratum</i>	FX	Fornix
UNC*	Uncinate fasciculus	TAP*	Tapetum
CP*	Cerebral peduncle	EC*	External capsule
ALIC*	Anterior limb of internal capsule	RLIC*	Retro-lenticular part of internal capsule
PLIC*	Posterior limb of internal capsule	FX/ST*	Fornix (cres) / Stria terminalis
CGH*	Cingulum (hippocampus)	SLF*	Superior longitudinal fasciculus
IFO*	Inferior fronto-occipital fasciculus	SFO*	Superior fronto-occipital fasciculus
SCR*	Superior <i>corona radiata</i>	CGC*	Cingulum (cingulate gyrus)

In addition, we computed whole-brain tractography using the DTIstudio program (<https://www.mristudio.org/>) and conducted cortical gray matter parcellation to yield 68 ROIs using Freesurfer (<http://surfer.nmr.mgh.harvard.edu/>) (**Table 2**). The gray matter parcellation was performed in the MPRAGE space, and the resulting ROI labels were registered to each subject's DTI space using affine transformations in FSL. For each pair of ROIs, the number of fibers connecting then determined the element in the corresponding connectivity matrix. These matrices can be analyzed using the Brain Connectivity Toolbox (<http://brain-connectivity-toolbox.net/bct>) to yield several graph theory metrics (density, strength, characteristic path length and global efficiency).

Table 2. 34 cortical labels per hemisphere were extracted as the basis for our 68x68 cortical connectivity matrices

1	Banks of the superior temporal sulcus	18	<i>Pars orbitalis</i>
2	Caudal anterior cingulate	19	<i>Pars triangularis</i>
3	Caudal middle frontal	20	Peri-calcarine
4	Cuneus	21	Postcentral
5	Entorhinal	22	Posterior cingulate
6	Fusiform	23	Pre-central
7	Inferior parietal	24	Precuneus
8	Inferior temporal	25	Rostral anterior cingulate
9	Isthmus of the cingulate	26	Rostral middle frontal
10	Lateral occipital	27	Superior frontal
11	Lateral orbitofrontal	28	Superior parietal
12	Lingual	29	Superior temporal
13	Medial orbitofrontal	30	Supra-marginal
14	Middle temporal	31	Frontal pole
15	Parahippocampal	32	Temporal pole
16	Paracentral	33	Transverse temporal
17	Pars opercularis	34	Insula

3. RESULTS AND DISCUSSION

As the FOV did not cover all structures below temporal lobes, only cerebral structures are considered. For standard FA, the following regions (-R and -L indicate right and left respectively) have significantly lower values in bipolar relative to healthy subjects: BCC ($p = .004$), SCC ($p = .025$) PCR-R ($p = .042$), SFO-L ($p = .036$), TAP-R ($p = .001$, and TAP-L ($p = .014$) On the other hand, GCC ($p = .025$), BCC ($p = .00025$), SCC ($p = .016$), PCR-L ($p = .045$), SLF-L ($p = .008$), TAP-R ($p = .012$), and TAP-L ($p = .03$) exhibited increased MD in bipolar relative to controls. For HARDI-corrected measures, GCC ($p = .045$), BCC ($p = .009$) SCC ($p = .017$), PLIC-R ($p = .044$), SFO-L ($p = .026$), TAP-R ($p = .004$), and TAP-L ($p = .032$) showed changes in HARDI-corrected FA. There were no significant differences in HARDI-corrected MD. Taken as a whole, only the corpus callosum (genu, body, and splenium) and bilateral tapetum (lateral extensions of the corpus callosum) exhibited changes in both DTI and HARDI corrected measures.[6] Controlling multiple comparisons across all measures using FDR (false discovery rate) at 0.05, only standard FA differences in the body of corpus callosum remained significant.

3.1. Investigating inter-hemispheric integration

Calculated by averaging the lengths of shortest paths between all pairs of nodes, the characteristic path length (CPL) [5] is commonly used to measure network integration. In our bipolar subjects, CPL values are significantly higher relative to controls (difference=0.008, $p=0.041$). The significantly higher CPL values in bipolar subjects thus indicate that information flow within the network is globally impeded compared to healthy subjects. However, a related global metric, the global efficiency (Eglob, the average inverse shortest length between all pairs of nodes) did not statistically differ between the two groups.

Moreover, the differences of CPL cannot be explained by fewer fiber tracts in bipolar subjects, as the two groups did not differ in density, degree, or strength.

Guided by these results, we further investigated the role of corpus callosum in the context of brain network analyses. We focused on the sub-network formed by the 68 cortical ROIs and created a “left-right” parcellation by dividing all cortical ROIs into those in the left versus right hemisphere. To measure the integration of left and right hemispheres, we first computed and compared, between groups, the mean participation coefficients [7] for each hemisphere (by averaging the participation coefficients of all nodes within the same hemisphere) based on this left-right parcellation. Given any pre-defined network parcellation, the participation coefficient of a node was originally proposed as a measure of the diversity of inter-modular connections for this node. Thus, if a node only directly connects with nodes within the same module, its participation coefficient is 0.

Modifying the definitions of CPL and Eglob, we proposed a set of four metrics to further probe modular integrations, which we term intra-/inter- modular path length and intra-/inter modular efficiency (intra-PL, inter-PL, E_{intra} , and E_{inter}). The intra-PL is computed using the mean within-module path length, averaged across all shortest paths connecting node pairs in the same module. On the other hand, inter-PL is numerically defined as the mean inter-modular distance (e.g., for module M_i and M_j , inter-PL is measured by averaging the path lengths of all shortest paths connecting any node in module M_i to any node in module M_j). In our case, as the brain parcellation only consists of left and right hemispheres, intra-PL (inter-PL) thus measures the mean path length when connecting any node to another node in the ipsilateral (contralateral) hemisphere. Mathematically, the intra-PL for module M_i is defined as:

$$\text{intra-PL}^{M_i} = \frac{\sum_{n, m \in M_i; n \neq m} d_{nm}}{\left(\{M_i\}^2 - \{M_i\}\right)/2}$$

Here $\{M_i\}$ denotes the number of nodes in module M_i , and d_{nm} denotes the length of the shortest path connecting nodes n and m . Similarly, the inter-PL between modules M_i and M_j is mathematically defined as:

$$\text{inter-PL}^{M_i \leftrightarrow M_j} = \frac{\sum_{n \in M_i; m \in M_j} d_{nm}}{\{M_i\}\{M_j\}}$$

In addition to inter- and intra- modular path length, we further propose the inter-modular and intra-modular efficiency as measures of network integration, mathematically defined as follows.

$$E_{\text{intra}}^{M_i} = \frac{\sum_{n, m \in M_i; n \neq m} d_{nm}^{-1}}{\left(\{M_i\}^2 - \{M_i\}\right)/2}; E_{\text{inter}}^{M_i \leftrightarrow M_j} = \frac{\sum_{n \in M_i; m \in M_j} d_{nm}^{-1}}{\{M_i\}\{M_j\}}$$

As the connectivity matrix measures the connectivity strength of graph edges, in order to construct the distance matrix (whose (i,j) -element denotes the length of the

shortest path connecting nodes i and j) a transformation on the connectivity matrix that relates the connectivity edge weights to edge “lengths” is needed (the “connectivity-to-length” mapping). Note that as a higher edge weight indicates stronger connectivity and a shorter edge length, this connectivity-to-length mapping usually takes the form of an “inverse” transformation. After applying the connectivity-to-length mapping to each subject’s structural connectivity matrix, we then use a weighted graph approach and construct the shortest path length using the well-known Dijkstra’s algorithm [8]. Two different connectivity-to-length mappings were explored in this study: 1) as the element-wise inverse, and 2) as the element-wise square root of the element-wise inverse of the connectivity matrix. Figure 2 shows the distance matrix from a control subject, elements of which indicate the shortest path length connecting node pairs.

Table 3 Inter-hemispheric path length and efficiency for the bipolar and healthy group (mean \pm standard variation; p values with * indicate reaching statistical significance at 0.05)

	Bipolar	Control	P value
Inter-hemispheric path length			
Inverse	0.096 \pm 0.028	0.082 \pm 0.028	0.08
Inverse-sqrt	0.490 \pm 0.049	0.445 \pm 0.063	0.006*
Inter-hemispheric efficiency			
Inverse	23.90 \pm 4.50	30.70 \pm 11.67	0.0091*
Inverse-sqrt	2.57 \pm 0.28	2.91 \pm 0.47	0.0035*

Our results showed that, given this left-right parcellation, our bipolar and control groups did not differ in the mean participation coefficients, E_{intra} or intra-PL for either the left or right hemisphere. By contrast, bipolar subjects exhibited significantly attenuated inter-hemispheric integration (lower inter-modular efficiency values) relative to normal control subjects regardless of the choice of the connectivity-to-length mapping, as well as longer inter-hemispheric path length when the element-wise inverse-square root mapping was applied (but no significant group difference in the case of element-wise inverse mapping). The results are summarized in **Table 3** and **Figure 1**.

4. CONCLUSION

We report the first neuroimaging study to map structural brain changes in euthymic bipolar subjects using brain network analyses coupled with state-of-the-art high angular resolution diffusion imaging. Our results revealed significantly altered white matter integrity in corpus callosum; this finding is then supported with subsequent brain network analyses showing deficits in inter-hemispheric integration in bipolar subjects relative to healthy controls. We also made technical contributions by introducing new metrics that probe inter-modular and intra-modular integration. These metrics can be applied given any sub-grouping of a network into a non-overlapping set of modules. Our results are scientifically relevant and may potentially have significant clinical implications.

Acknowledge: This study was funded by grants from the National Alliance for Research on Schizophrenia and Depression (NARSAD-G5749; Leow), and the National Institute of Mental Health (NIMH-1R21MH086104; Altshuler).

5. REFERENCES

[1] Bellani M. and Brambilla P. “Diffusion imaging studies of white matter integrity in bipolar disorder,” *Epidemiol Psychiatr Sci.* 20(2):137-140.(2011)

[2] Bellani M., Yeh PH., Tansella M., Balestrieri M., Soares JC., Brambilla P. “DTI studies of corpus callosum in bipolar disorder.” *Biochemical Society Transactions.* 37: 1096-1098. (2009)

[3] Heng S., Song AW., Sim k. “White matter abnormalities in bipolar disorder: insights from diffusion tensor imaging studies. “ *J. Neural Transm.* 117 (5):639-654. (2010)

[4] Leow AD., Zhu S., Zhan L., McMahon K., de Zubicaray GI., Meredith M., Wright MJ, Toga AW., Thompson PM. “The tensor distribution function. “ *Magn Reson Med.* 61(1):205-214. (2009).

[5] Watts D.J., Strogatz S.H. “Collective dynamics of small world networks.” *Nature.* 393: 440-442. (1998)

[6] Zhan L, Leow AD, Zhu S, Hageman N, Chiang MC, Barysheva M, Toga AW, Thompson PM. "A novel measure of fractional anisotropy based on the Tensor Distribution Function". MICCAI2009, London, UK. (2009).

[7] Guimera, R, Amaral, LAN. “Functional cartography of complex metabolic networks.” *Nature.* 433: 895-900. (2005)

[8] Dijkstra EW. “A note on two problems in connexion with graphs.” *Numerische Mathematik.* 1: 269–71. (1959)

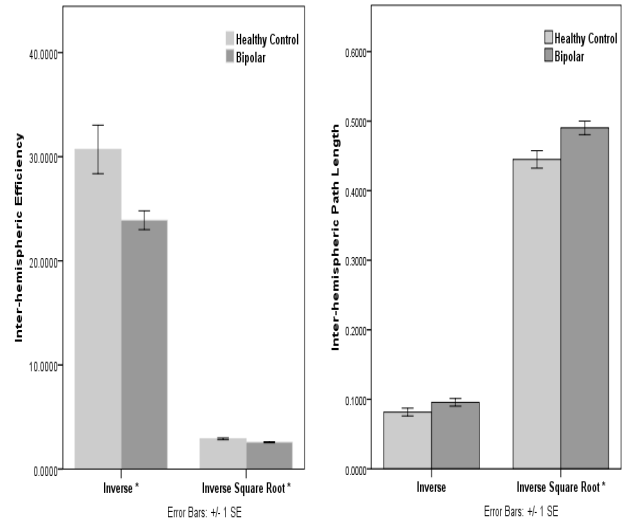


Fig.1. Inter-hemispheric efficiency (left panel) and inter-hemispheric path length (right panel) in bipolar versus healthy subjects (comparisons reaching statistical significance are indicated with *). To compute shortest path lengths, two definitions of connectivity-to-length mappings are explored: the inverse and the inverse square root mapping. The results showed that bipolar subjects on average have significantly lower inter-hemispheric efficiency (for both mappings), and a significantly longer inter-hemispheric path length when the inverse square root mapping is used.

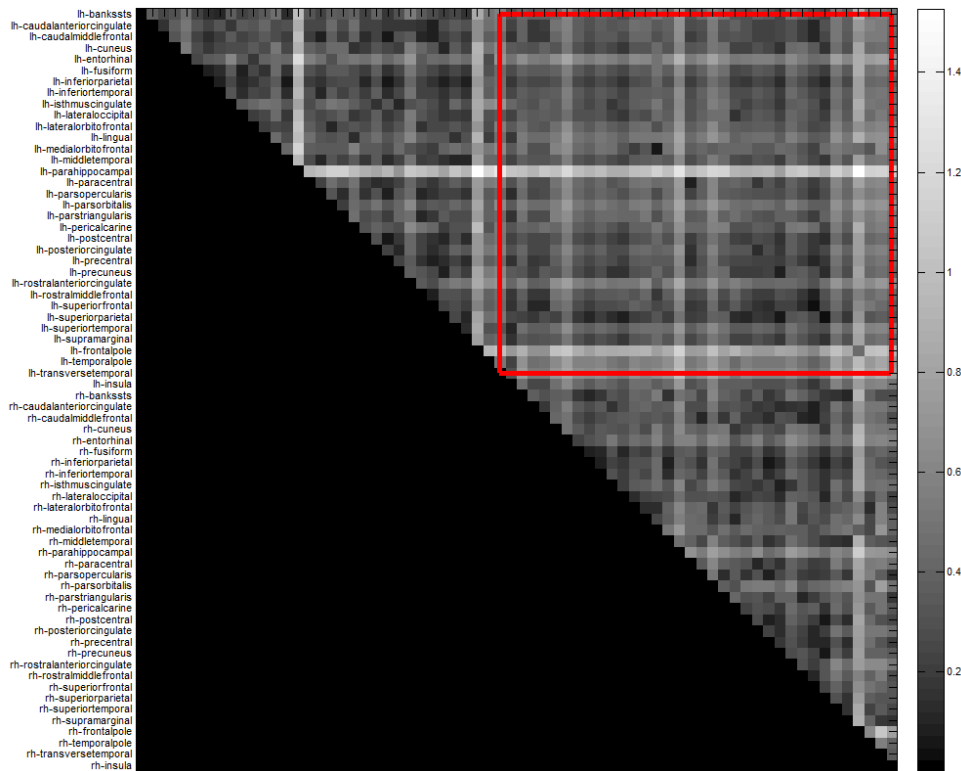


Fig.2. The distance matrix from a normal subject, elements of which indicate the shortest path length connecting node pairs. Only upper-diagonal part is shown as the matrix is symmetrical. In this example, the element-wise inverse of the element-wise square root mapping is used. Elements in red indicate inter-hemispheric connections.